Title: Development of a novel connectivity-based electric-field modelling approach for individualized targeting of transcranial magnetic stimulation treatment

Running title: Novel modelling approach for individualized TMS targeting

Authors: Nicholas L Balderston[1], Darsol Seok[1], Walid Makhoul[1], Zhi-De Deng[2], Tommaso Girelli[1], Marta Teferi[1], Nathan Smyk[1], Marc Jaskir[1], Desmond J Oathes[1], & Yvette I Sheline[1]

1. Center for Neuromodulation in Depression and Stress
Department of Psychiatry
University of Pennsylvania
Philadelphia, PA, USA

2. Noninvasive Neuromodulation Unit
National Institute of Mental Health
Bethesda, MD, USA

Corresponding Author:
Nicholas Balderston
Center for Neuromodulation in Depression and Stress
3700 Hamilton Walk, Richards D302
Philadelphia, PA, 19104
Phone: 215-746-3058
Fax: 215-573-8556
nicholas.balderston@pennmedicine.upenn.edu

Keywords: Transcranial Magnetic Stimulation, resting state, functional connectivity, electric field modelling, depression, anxiety, anxious misery

Abstract

Background

Resting state functional connectivity (rsFC) offers promise for individualizing stimulation targets for transcranial magnetic stimulation (TMS) treatments. However current targeting approaches do not account for non-focal TMS effects or large scale connectivity patterns. To overcome these limitations, we propose a novel connectivity-based electric-field (e-field) modelling approach to identify optimal single-subject TMS targets using whole-brain rsFC.

Methods

We recruited 91 anxious misery (AM) patients and 25 controls. We measured depression symptoms via standard clinical questionnaires (MADRS/HAMD) and via a data-driven symptom clustering approach (Loss cluster) which used multiple items across 32 clinical measures. We also recorded rsFC in these individuals. We then used a Principal components analysis (PCA) regression to predict symptoms from rsFC and generate a slope vector (M) and intercept (b) for our e-field augmented model. We modeled 17 left dlPFC sites using 24 equally spaced coil orientations. We computed single-subject predicted ΔMADRS/HAMD and Δ Loss scores for each site/orientation combination according to the following equations: $\Delta MADRS/HAMD = MEX + b$, and $\Delta\ Loss = MEX + b$, where E represents a vectorized summary of the e-field model an X represents the single-subject rsFC matrix.

Results

In AM patients, our model predicted a significant decrease in depression symptoms (measured by both MADRS/HAMD and Loss cluster) near BA46 for coil orientations perpendicular to the cortical gyrus. In control subjects, no site/orientation combination showed a significant relationship with MADRS/HAMD or Loss symptoms.

Discussion

These results replicate previous work demonstrating the efficacy of left dlPFC stimulation for depression treatment, and predict maximal efficacy near BA46. Importantly, our novel connectivity-based e-field modelling approach predicted a significant decrease in depression symptoms with more focal effects seen for the Loss cluster, and may be an effective way to identify potential TMS treatment responders, as well as to individualize TMS targeting to maximize the therapeutic impact.

Introduction

Major depressive disorder (MDD) is a mood disorder characterized by depressed mood or loss of interest or pleasure (1). Symptoms include feelings of worthlessness; indecisiveness or difficulty concentrating, change in weight, appetite, and sleep; psychomotor agitation; and suicidal ideation (1). According to the World Health Organization (WHO) World Mental Health (WMH) Surveys Initiative (2), lifetime prevalence rates within the United States average 16.9%, with women showing higher prevalence than men (20.2% vs. 13.2%) (2). The most common treatments for MDD include antidepressant medication, psychotherapy/cognitive behavioral therapy (CBT), or a combination of the two (https://www.nimh.nih.gov/health/statistics/major-depression.shtml). Although antidepressant use is prevalent, there are reports of mixed efficacy. TMS to the left dlPFC has been approved by the FDA, and has been shown to be effective as an antidepressant treatment in treatment resistant depression, or in a patient population that have not responded to or tolerated previous antidepressant medication trials (3–5). Although many studies find a significant reduction in depressive symptoms (6–12), there have also been studies finding limited efficacy of TMS for major depression (13, 14), leaving room for improvement.

One possible explanation for the heterogeneity in TMS treatment response for major depression is that the standard scalp-based targeting approach (i.e. the 5cm rule) does not account for individual variations in cortical anatomy, and often selects regions outside the dlPFC, which may explain some of the modest therapeutic effects (15). Image-guided TMS incorporating MRI-neuronavigation, taking into account individual differences in brain anatomy, can target specific functional brain networks with greater precision. Using structural MRI to locate a specific site at the junction of BA 9 and 46 has shown greater efficacy than the traditional 5-cm rule (14). More recent approaches have used functional MRI (fMRI) to target

regions dlPFC that are downstream of the dlPFC, like the subgenual anterior cingulate cortex (sgACC) that are thought to be dysfunctional in MDD patients (16–19). Key to this approach is to use functional connectivity of the downstream site to identify the dlPFC site with the strongest connectivity.

Although this connectivity-based approach represents the current cutting-edge in the field, and is an improvement on the standard scalp-based targeting approach used clinically, it has two fundamental limitations. First, focusing on a single downstream region to define the TMS target does not account for off-target effects in other downstream regions. Second, although there may be ample evidence associating the downstream target with symptoms, there is no guarantee that the net effects of the TMS will move symptoms in the desired direction. To address these limitations, we developed a novel computational model based on whole brain functional connectivity and electric-field modelling. To address the first limitation, we use electric-field modelling to estimate the change in connection strength across the whole brain given a particular site and orientation of stimulation. To address the second limitation, we use multiple linear regression to estimate the net effects of these connection strength changes on symptoms. The overall concept is to generate a predicted symptom change score following neuromodulatory TMS at a particular site and stimulation. We then iterate the model across sites and orientations to find the site/orientation combination that leads to the maximal reduction in MDD symptoms.

Materials and Methods

Participants

One hundred eighteen participant (Age: M=28.42, SD=7.92) entries were pulled from the Dimensional Connectomics of Anxious Misery dataset (20), and included anxious misery

participants (93 total, 64 were females) and healthy controls (25 total, 16 were females; See Table 1). Mean age of the anxious misery cohort was M=28.29 (8.2) and of healthy controls M=28.92 (6.91). Patients included in the anxious misery cohort were selected on the basis of their score on the NEO Five-Factor Inventory (NEO FFI) (21) rather than on diagnosis in keeping with the RDoC concept of finding symptom domains across diagnoses. In post-hoc analyses, the anxious misery cohort included a range of different primary diagnoses, namely major depressive disorder (N = 41), persistent depressive disorder (N = 9), social anxiety disorder (N = 5), generalized anxiety (N = 21), and PTSD (N = 17).

Basic Inclusion/Exclusion criteria included MRI contraindications, histories of certain neurological or cognitive disorders and events, histories of exclusionary psychiatric conditions or any other factors that may have affected patient safety (See Seok et al. (20) for complete list). In addition, participants in the anxious misery cohort needed to score a minimum of one (1) standard deviation above a point estimate of the general adult population mean (distributions for males and females were different) in the NEO FFI (21) in order to be included in the study (20). Conversely, healthy controls needed to score one (1) standard deviation or more below the mean point estimates to be eligible to participate. Subject were recruited by means of IRB-approved advertisement and phone calls. All participants signed an informed consent form, and the protocol was approved by the Institutional Review Board for human subject research at the University of Pennsylvania.

Procedure

On the initial visit, written consent was obtained from all eligible participants prior to enrolling in the study, followed by a baseline visit with study staff to ascertain their medical history and demographic information. In addition, a research version of the Structured Clinical

Interview for DSM-5 (SCID-5-RV) (1) was conducted by a trained member of the staff to document their psychiatric diagnosis and history, and the remaining assessments (See Below) were conducted. In a follow-up visit, a 2-hour fMRI scan was conducted, where structural, diffusion, resting state, and task-based fMRI were collected as part of the larger project.

Assessments

Many clinical measures were used to identify the behavioral and cognitive features of anxious misery. In this project, eligible participants completed 17 self-report and 3 clinician-administered measures. The clinician-administered measures include the Montgomery-Asberg Depression Rating Scale (MADRS) (22) and the Hamilton Depression Rating Scale (HAMD) (23) in order to assess depression severity.

Symptom Clustering

In addition to scores on the HAMD and MADRS which are strongly correlated (AM, r = 0.857; Control, r = 0.664), we used a Loss (depression) cluster from our questionnaire data that is consistent with the Loss construct in the NIMH RDOC matrix (24, 25). We applied a standard community detection algorithm (Louvain modularity, gamma = 1) on the Pearson correlation matrix of our 141 items from 8 negative valence instruments MADRS, HAMD, Snaith-Hamilton Pleasure Scale (SHAPS) (26), Mood and Anxiety Symptom Questionnaire (MASQ) (27), CTQ (28), Insomnia Severity Index (ISI) (29, 30), RTS (31) and Anxiety Sensitivity Index (ASI) (32). This generated five distinct clusters of behavioral features, one of which contained items that primarily indexed the Loss construct of the Negative Valence domain. Finally, to quantify each individual's degree of Loss, we z-scored each item across the AM group so that each item had a mean of 0 and a variance of 1 and then took the mean across every z-transformed item in the

Loss cluster. The final result is a single score representing each participants' degree of Loss relative to the rest of our AM sample.

MRI Scans

MRI data was acquired as part of the Dimensional Connectomes of Anxious Misery project (20), one of the Connectomes Related to Human Diseases (CRHD) studies (https://www.humanconnectome.org/disease-studies). Accordingly, data acquisition and scanning parameters were designed to be harmonized with three other CRHD studies: the Mapping Connectomes for Disordered Mental States (33), the Boston Adolescent Neuroimaging of Depression and Anxiety study (34) and the Treatment of Resistant Depression Connectome by Fast-Acting Therapies (35).

Participants were scanned on a Siemens Prisma 3T using a 64-channel head coil. Structural T1-weighted images were acquired using a magnetization-prepared rapid acquisition with gradient echo (MPRAGE) sequence with TR=2400ms, TE=2.22ms and flip angle of 8 degrees. 208 slices were acquired with a voxel resolution of 0.8mm isometric, resulting in an FOV of 256 x 240 x 167mm. T2-weighted images were acquired using a variable-flip-angle turbo-spin echo (TSE) sequence with TR=3200ms and TE=563ms, with the same voxel resolution and FOV as the T1w acquisition. Resting state fMRI data were acquired with a multi-band acceleration of 8, TR=800ms, TE=37ms and flip angle of 52 degrees. Whole-brain coverage was achieved with 72 slices and a voxel resolution of 2.0mm isometric, resulting in an FOV of 208 x 208 x 144mm. Each resting state scan was paired with another run with the opposite phase encoding direction (AP-PA), and two such pairs were acquired, resulting in 22:24 minutes of data (5:46 min x 4 runs) for each participant. Spin echo field maps were also acquired in opposite phase encoding directions in order to correct susceptibility distortions. During the

resting state scan, participants were shown a white screen with a black crosshair in the center and were instructed to remain still with their eyes open and to blink normally.

MRI preprocessing

Computational head modelling for e-field calculations. We used the SimNibs software package to generate 3D head and coil geometries using the finite element method (FEM) (36). T1 and T2 structural MRIs were combined to create an individualized head model and then segmented into scalp, skull, CSF, gray matter, and white matter volumes. These volumes were then converted to tetrahedral meshes using a Gmsh subroutine packaged in SimNIBS (37).

E-field calculations. E-field models were conducted for each site/orientation combination (See Below), and the magnitude of the normal component of the electric field at each surface node was used to model the potential TMS effects (38).

fMRI preprocessing

Data were preprocessed using the Human Connectome Project Pipelines v4.0.1 (retrieved from https://github.com/Washington-University/HCPpipelines/releases/tag/v4.0.1). A full description of preprocessing steps is provided elsewhere (39). In brief, anatomical preprocessing steps included gradient nonlinearity distortion correction, co-registration of T1w and T2w images, bias-field correction using spin-echo field maps and spatial normalization to the Montreal Neurological Institute (MNI) template. Functional image preprocessing steps included removal of spatial distortions via gradient nonlinearity corrections, correction of participant motion through volume realignment, susceptibility distortion correction using dual-phase encoded spin-echo corrections, registration of fMRI data to T1 space, subsequent transformation to MNI-space and removal of extra-parenchymal voxels.

Timeseries analyses using volumetric data were further conducted using the eXtensible

Connectivity Pipeline (XCP Engine) (40). The workflow is summarized as follows: (i) removal of the 10 initial volumes (8 seconds) to achieve signal stabilization, (ii) demeaning and removal of quadratic trends using a general linear model to account for scanner drift, (iii) intensity despiking using 3dDespike from AFNI (41), (iv) bandpass temporal filtering of time series between 0.01 Hz and 0.08Hz using a first-order Butterworth filter (42), (v) regression of nine confounding signals (six motion parameters + global signal + mean white matter signal + mean cerebral spinal fluid signal) and as well as the temporal derivative, quadratic term and temporal derivatives of each quadratic term (resulting in 36 regressors total) (43), and (vi) spatial smoothing with SUSAN from FSL (44) using a 6mm FWHM kernel. Voxelwise timeseries were then downsampled to the 333 parcels in the Gordon atlas (45) and NxN connectivity was calculated using Z-tranformed Pearson correlations.

Model steps

PCA regression. For the first step in our analysis (See Figure 2 and Appendix for detailed equations), we used principal components analysis (PCA) regression to model the relationship between functional connectivity and symptoms (46, 47). We began by conducting a principal components analysis on the functional connectivity data to reduce noise and minimize collinearity (48). We restricted attention to the subset of components that explained largest proportions of variability, with the assumption that these contain most of the signal. For this we used a geometric approach that identified the eigenvalue at the elbow of the scree plot (i.e. the eigenvalue furthest from the hypotenuse connecting the first and last eigenvalues). The principal component scores for each of these components were then used to model symptom scores in a multiple linear regression. The resulting beta coefficients were then vectorized and combined with the principal component coefficients using matrix multiplication. The result was an item-

length vector where the value at each point represented the overall variability in symptoms accounted for by that particular functional connection.

Selection of sites and orientations. A series of 17 sites along the anterior-to-posterior gradient of the L DLPFC were used in the model (See Supplemental Table 1). This site vector was anchored by 3 therapeutic sites described in (49) ([-41, 16, 54] based on 5cm rule, [-36, 39, 43] BA9, [-44, 40, 29] BA46), and extends 12 mm posterior to the 5mm site and 12 mm anterior to the BA46 site. At each site, we generated 24 different e-field models. For each model, the roll and pitch of the TMS coil was defined perpendicular to the scalp. The yaw vector was selected from 24 possible orientation vectors spaced at 15-degree increments.

E-field connectivity matrices. The e-field maps were downsampled (i.e. averaged across voxels in each parcel) to the Gordon atlas (45), converted to a 1 x 333 vector, and thresholded using the same geometric approach described in the PCA regression section (See Figure 3 and Appendix for detailed equations). To estimate how stimulation at a specific site and orientation might affect connectivity, the downsampled e-field vector was used to form an NxN matrix where the values in the matrix represent the average current induced in the ROIs for each connection.

E-field/connectivity symptom estimates

The predicted neuromodulatory effect of TMS on symptoms was modelled using the e-field model matrix, the single-subject connectivity matrix, and the estimated group-level coefficients derived from the symptom/connectivity regression, according to the equation in Figure 1B. These calculations were iterated across all sites and orientations to create the heatmap shown in Figure 4, where each value in the heatmap represents the predicted change in symptoms for that subject given hypothetical TMS administered at that particular site and

orientation.

Statistical analysis

To determine whether our novel modelling approach predicted significant changes at the group level, we conducted one-sample t-test of the predicted change in symptoms (i.e. baseline symptom – predicted post treatment symptom) against zero. A significant negative t-score would indicate a predicted decrease in symptoms at the group level. We repeated this process for all site/orientation combinations, and generated heatmaps from the resulting t-scores. To correct for multiple comparisons across site and orientation, we conducted 10,000 permutations where the sign of the symptom – predicted symptom change was randomly flipped across subjects and permutations. T-scores were then calculated at each site/orientation combination within the permuted heatmap. The maximum t-score from each permuted heatmap was then extracted and used to build a null distribution. We used a 2-tailed alpha of 0.05, and thus selected the critical values correspond to the 2.5^{th} and 97.5^{th} percentiles of the null t-score distribution generated from the permutation procedure. Accordingly, the null hypothesis for each site/orientation combination is that the model predicts no significant change in symptoms following a hypothetical treatment at that site/orientation. The heatmap from the actual test was then thresholded using these t-score critical values (See Table 2 for values).

Results

PCA regression

Separate PCA/regression analyses were conducted for the anxious misery group and the control subjects. For the AM group, 11 signal components were selected, and these components explained 31% of the variability in the functional connectivity signal. For the control group, 6

components were selected, and these components explained 40% of the variability in the functional connectivity signal.

Individual subject predictions

One goal of this project was to determine whether the modelling approach above could be used to make targeting decisions for the application of TMS to single subjects. Accordingly, reliable single subject data is key to achieving this goal. Single subject heatmaps from the AM group show clear systematic patterns of predicted symptom change as a function of both site and orientation (See Figure 5), suggesting that this modelling approach can be used to simultaneously optimize these two parameters at the single subject level. These patterns are characterized by punctate “cool spots” in the heatmap that identify a clear site/orientation combination that yields maximal symptom reduction. The overall pattern of results is consistent across the MADRS, HAMD, and Loss heatmaps. Furthermore, consistent with previous literature on remission rates following therapeutic rTMS, our model predicts a reduction in MADRS scores in approximately two-thirds of the patients (n = 59/90) if we extract the predicted MADRS score at the site/orientation combination (5cm anterior to MT at ~45 degrees eccentricity) typically used for therapeutic rTMS. Using our approach to optimize site and orientation results in a modest increase in predicted responders (n = 66/90). Importantly, this pattern seems to be specific to those in the AM group as control subjects do not show the characteristic “cool spots” in their heatmaps (See Figure 6).

Group level predictions

To determine whether the model made significant predictions at the group level, we calculated the predicted change in depression symptoms for each site/orientation combination by subtracting the predicted MADRS/HAMD and Loss scores (i.e. values in Figure 5) from the

observed MADRS/HAMD and Loss scores. These difference scores represent the predicted change in depression symptoms, given a specific site/orientation of stimulation. We then compared these values to 0 (i.e. no effect of TMS) using a single sample t-test. We corrected for multiple comparisons across sites/orientations using permutation tests. As shown in Figure 7 our model predicts a significant decrease in MADRS, HAMD, and Loss scores in AM subjects with both left and right dlPFC stimulation. In the left hemisphere, the cool spots are centered on BA46 at 30-45 degrees orientation. In the right hemisphere, the cool spots are positioned slightly anterior to BA46, and strongest at 120 and 135 degrees orientation, roughly perpendicular to the optimal coil angle in the left. Consistent with the results at the single-subject level, these results suggest that there is a significant relationship between both site and orientation and predicted symptom change. In addition, the results from the Loss cluster are much more focal than the results from either the MADRS or the HAMD, suggesting that the item clustering approach may lead to more specific targeting results. Importantly, these results are limited to the AM subjects, as the model predicts no significant changes in depression symptoms in the healthy control subjects (See Figure 8).

Discussion

Here we present a proof of concept methodological study where we use functional connectivity and electric-field modelling to predict symptom change following a hypothetical course of neuromodulatory treatment with TMS. Our model calculates the relationship between symptoms and connectivity, as well as the effect of TMS on connectivity to yield a predicted change score in the symptom, assuming TMS is delivered at the site and orientation specified in the model. By iterating this process across sites and orientations, we are able to show a systematic effect of both site and orientation on predicted treatment outcome, as measured by

MADRS, HAMD, and Loss scores, with more focal effects seen for Loss. Importantly, these effects are apparent at both the single-subject and the group level, suggesting that this approach has sufficient power to identify subject-specific TMS targets to maximize symptom reduction.

Consistent with previous work implicating the junction of BA9 and BA46 as a potentially optimal site of stimulation for depression symptoms (50–54), we show with both MADRS and HAMD scores that are model predicts the largest symptom reduction at this location (55). Our model adds to the work suggesting that targeting rsFC networks can inform TMS targeting (56), and are consistent with the findings that individualized rsFC maps may be most informative (49). Previous research has shown that regions of the dlPFC that are more strongly anticorrelated with sgACC tend to show better clinical efficacy when targeted with therapeutic TMS (50, 57), and the closer the stimulation site is to this optimally anticorrelated dlPFC location, the better the clinical outcome (53, 54, 58). Importantly, active rTMS to the l dlPFC has been shown to reduce anticorrelation between the dlPFC and sgACC (52, 59, 60), and prospective targeting based on individualized dlPFC sgACC connectivity leads to a greater reduction in symptoms compared to traditional targeting (52, 53). In addition, there is some research to suggest that individualized targeting of BA46 through a parcel guided approach can improve treatment response in patients who have previously failed standard TMS targeted at the dlPFC using the 5CM rule (55). Based on this work, it could be argued that the current state-of-the-art for individualized TMS targeting for depression is to target sites in the left dlPFC with maximal connectivity with the subgenual cingulate cortex.

However, a review of 33 studies with pre-post resting state shows that although TMS induces robust changes in rsFC, the majority of effects are outside of the stimulated functional network (61). Indeed, the changes in functional connectivity following rTMS treatment for

depression can be seen throughout the brain in regions that are important for affective responding (e.g. insula, amygdala, inferior parietal lobule, etc.), suggesting that the net effects on symptoms may be driven by these large scale network connectivity changes (62). Consistent with this idea, treatment response has also been linked to rsFC changes outside of the sgACC (63, 64). Together these results suggest that a whole brain connectivity model may outperform single connection targeting approaches, like the ones described above.

In keeping with these results, our whole brain connectivity approach has several potential benefits over single connection targeting approaches (50–54). First, our model uses e-field modelling to account for the variability in electric current spread due to individual differences in cortical anatomy, and uses this information to inform targeting. Second, our approach accounts for other connections in the brain that 1) may be impacted by TMS treatment, and 2) contribute to symptom reduction. Importantly, our model uses a data driven approach to weight these connections by the amount of variability they explain in the depression symptoms. Finally, our approach uses agnostic data-driven estimates between behavioral characteristics and functional connectivity to drive targeting. Therefore, this model can be extended to other symptoms/behavioral characteristics where reliable measures of behavioral markers are available (e.g. addiction, anxiety, etc.).

The main focus of the paper was depressive symptoms, which we captured using scores on the MADRS and HAMD as well as the data-derived Loss cluster. However it is important to note that the model described here can be applied to other symptom measures as well. As described above, we have used various symptom clustering approaches to extract distinct symptom measures from available clinical data (65), resulting in several distinct symptom clusters. Although out of the scope of the current work, future studies should determine the

degree to which these other distinct symptom clusters could potentially be used to direct TMS targeting. Indeed, defining biotypes for depression and anxiety starting with neural circuit dysfunction (66), may yield additional symptom-specific targets. Consistent with this idea, the results from the Loss cluster were more focal than the results using the clinical scores, suggesting that the major symptoms that contribute to the overall clinical presentation of depression may have their own unique optimized TMS target. Accordingly, the model presented here could be used not only to individualize targeting at the single subject level, but it could potentially be extended to individualize targeting at the single session level, where each TMS session in a course of treatment is targeted at a specific symptom or set of symptoms, thereby maximizing the therapeutic effect.

Strengths and Limitations

The strength of the work describe here stem from the generality of its applicability. The model described in this work is both site and symptom independent. Therefore, the methods described here can be used to optimize TMS targeting for a variety of disorders shown to be effectively treated with TMS (67). In addition, this approach could be used prospectively to screen for potential TMS effects within new disorders or for novel symptom dimensions. In addition, the model is able to make predictions at the single-subject level regarding the optimal stimulation site for a given symptom, allowing for single-subject optimization of TMS targeting. In all cases, the predictions of the model can be directly tested by applying TMS according to the model predictions.

The primary weakness of this study is that it is a proof of concept study, rather than a confirmatory study, meaning we do not actually administer TMS and measure the pre/post symptom changes in the current work. We understand that this is the necessary next step to

validate the current model. Our hope is that publishing the model in its initial state will allow multiple labs to test the predictions of the model, allowing for a more rapid validation/refinement of the work. To facilitate this process, we plan to make the code for our model publicly available.

Another potential weakness of the current work is that we used Pearson's correlations, a non-directional measure, to model functional connectivity. However, it is likely that TMS affects upstream and downstream connections differentially (68). Accordingly, it may be more appropriate to model the functional connections using effective connectivity, and differentially weight the connections based on whether they are upstream or downstream of the stimulation site. Of course this becomes more complicated in our model, given that the stimulation "site" is modelled as a thresholded map of the current induced across the whole brain, given a TMS coil position and orientation. Accordingly, to factor in differential effects for upstream and downstream connections, it would be necessary to generate an NxN effective connectivity map of the entire brain. While techniques like dynamic causal modelling (DCM) can be used to generate realistic effective connectivity models with a limited number of sites and connections (69–71), it remains to be seen whether this approach can be reliably used to generate whole brain effective connectivity models for use at the single-subject level (72).

One final weakness of the current work is that the model assumes that changes in connectivity scale with the magnitude of the electric field induced, given a particular site/orientation of stimulation. This assumption likely holds for little if any *in vivo* applications of TMS. Indeed, it is well known that the effects of TMS on outcome variables like cortical excitability (73, 74), functional connectivity (52, 60), and behavior (75, 76) are dependent on the stimulation parameters used (61, 77). Indeed, amplitude (78), frequency (79), pattern (80), number of sessions (5), and intervals (80) between sessions are all known to be important

determinants of observed TMS effects. We understand that the linear assumption put forth in our model is a massive oversimplification, but we see this as a starting point. Our goal is to state the initial model as parsimoniously as possible, to allow the model to be tested with a variety of experimental and clinical TMS protocols.

Conclusions

Individualized targeting is one key to maximizing the efficacy of clinical rTMS, and mapping TMS-induced changes in rsFC to changes in clinical symptoms is critically important for this goal. The model proposed here accomplishes this goal in a manner that is both site and symptom independent. We have validated the model using depression symptoms in a cohort of anxious misery patients, and shown that it replicates the finding that BA46 (an area with strong sgACC anticorrelation) may be maximally effective for treating depression (50–54). However, it is our hope that this work will be applied more generally to optimize TMS targeting across psychiatric disorders.

Author contributions: NLB: Designed Study, Conducted analysis, wrote manuscript, provided supervision, edited manuscript. **DS:** Assisted with data collection and preprocessing. **WM:** Assisted with data collection and preprocessing. **JB:** Conducted statistical analysis; edited manuscript. **ZD:** Assisted with statistical analysis and manuscript preparation. **TG:** Assisted with data collection and preprocessing,. **MT:** Assisted with data collection and preprocessing, assisted with manuscript preparation. **NS:** Assisted with data collection and preprocessing. **MJ:** Assisted with data collection and preprocessing. **DJO:** Assisted with study design; edited manuscript. **RTS:** Assisted with statistical analysis; edited manuscript. **YIS:** Assisted with study design, wrote manuscript; provided supervision; edited manuscript.

Acknowledgments: This study utilized the high-performance computational capabilities of the Cubic computing cluster at the University of Pennsylvania. (https://www.med.upenn.edu/cbica/cubic.html). The authors would like to thank Maria Prociuk for her expertise and assistance in submitting the manuscript. We would also like to thank the participants for their time and effort.

Financial Support: This project was supported in part by a 2018 NARSAD Young Investigator Grant from the Brain & Behavior Research Foundation (NLB); and by a K01 award K01MH121777 (NLB). Financial support for this study was provided by U01MH109991 (YIS) and by an endowment (YIS).

Ethical Standards: The authors assert that all procedures contributing to this work comply with the ethical standards of the relevant national and institutional committees on human experimentation and with the Helsinki Declaration of 1975, as revised in 2008.

References

1. American Psychiatric Association (2013): *Diagnostic and Statistical Manual of Mental Disorders: Dsm-5*. Diagnostic and Statistical Manual of Mental Disorders. Arlington, VA: Amer Psychiatric Pub Incorporated. Retrieved from http://books.google.com/books?id=EIbMlwEACAAJ.

2. Scott KM, de Jonge P, Stein DJ, Kessler RC (2018): *Mental disorders around the world: Facts and figures from the WHO World Mental Health surveys*. *Ment Disord Around World Facts Fig from WHO World Ment Heal Surv*. . doi: 10.1017/9781316336168.

3. McClintock SM, Reti IM, Carpenter LL, McDonald WM, Dubin M, Taylor SF, *et al.* (2018): Consensus recommendations for the clinical application of repetitive transcranial magnetic stimulation (rTMS) in the treatment of depression. *J Clin Psychiatry*. . doi: 10.4088/JCP.16cs10905.

4. Conelea CA, Philip NS, Yip AG, Barnes JL, Niedzwiecki MJ, Greenberg BD, *et al.* (2017): Transcranial magnetic stimulation for treatment-resistant depression: Naturalistic treatment outcomes for younger versus older patients. *J Affect Disord*. . doi: 10.1016/j.jad.2017.03.063.

5. O'Reardon JP, Solvason HB, Janicak PG, Sampson S, Isenberg KE, Nahas Z, *et al.* (2007): Efficacy and Safety of Transcranial Magnetic Stimulation in the Acute Treatment of Major Depression: A Multisite Randomized Controlled Trial. *Biol Psychiatry*. 62: 1208–1216.

6. Philip NS, Aiken EE, Kelley ME, Burch W, Waterman L, Holtzheimer PE (2019): Synchronized transcranial magnetic stimulation for posttraumatic stress disorder and comorbid major depression. *Brain Stimul*. . doi: 10.1016/j.brs.2019.06.010.

7. Clarke E, Clarke P, Gill S, Paterson T, Hahn L, Galletly C (2019): Efficacy of repetitive

transcranial magnetic stimulation in the treatment of depression with comorbid anxiety disorders. *J Affect Disord*. . doi: 10.1016/j.jad.2019.03.085.

8. Kumar S, Singh S, Parmar A, Verma R, Kumar N (2018): Effect of high-frequency repetitive transcranial magnetic stimulation (rTMS) in patients with comorbid panic disorder and major depression. *Australas Psychiatry*. . doi: 10.1177/1039856218771517.

9. Philip NS, Ridout SJ, Albright SE, Sanchez G, Carpenter LL (2016): 5-Hz Transcranial Magnetic Stimulation for Comorbid Posttraumatic Stress Disorder and Major Depression. *J Trauma Stress*. . doi: 10.1002/jts.22065.

10. Gwynette MF, Lowe DW, Henneberry EA, Sahlem GL, Wiley MG, Alsarraf H, *et al.* (2020): Treatment of Adults with Autism and Major Depressive Disorder Using Transcranial Magnetic Stimulation: An Open Label Pilot Study. *Autism Res*. . doi: 10.1002/aur.2266.

11. Mantovani A, Aly M, Dagan Y, Allart A, Lisanby SH (2013): Randomized sham controlled trial of repetitive transcranial magnetic stimulation to the dorsolateral prefrontal cortex for the treatment of panic disorder with comorbid major depression. *J Affect Disord*. 144: 153–159.

12. White D, Tavakoli S (2015): Repetitive transcranial magnetic stimulation for treatment of major depressive disorder with comorbid generalized anxiety disorder. *Ann Clin Psychiatry*. 27: 192–196.

13. Thompson L (2020): Treating major depression and comorbid disorders with transcranial magnetic stimulation. *J Affect Disord*. 276: 453–460.

14. Fitzgerald PB, Maller JJ, Hoy KE, Thomson R, Daskalakis ZJ (2009): Exploring the optimal site for the localization of dorsolateral prefrontal cortex in brain stimulation experiments. *Brain Stimul*. . doi: 10.1016/j.brs.2009.03.002.

15. Fitzgerald PB, Hoy K, McQueen S, Maller JJ, Herring S, Segrave R, *et al.* (2009): A randomized trial of rTMS targeted with MRI based neuro-navigation in treatment-resistant depression. *Neuropsychopharmacology*. . doi: 10.1038/npp.2008.233.

16. Hamani C, Mayberg H, Stone S, Laxton A, Haber S, Lozano AM (2011): The subcallosal cingulate gyrus in the context of major depression. *Biol Psychiatry*. . doi: 10.1016/j.biopsych.2010.09.034.

17. Mayberg HS, Lozano AM, Voon V, McNeely HE, Seminowicz D, Hamani C, *et al.* (2005): Deep brain stimulation for treatment-resistant depression. *Neuron*. . doi: 10.1016/j.neuron.2005.02.014.

18. Mayberg HS, Brannan SK, Mahurin RK, Jerabek PA, Brickman JS, Tekell JL, *et al.* (1997): Cingulate function in depression. *Neuroreport*. . doi: 10.1097/00001756-199703030-00048.

19. Drevets WC, Savitz J, Trimble M (2008): The subgenual anterior cingulate cortex in mood disorders. *CNS Spectr*. . doi: 10.1017/S1092852900013754.

20. Seok D, Smyk N, Jaskir M, Cook P, Elliott M, Girelli T, *et al.* (2020): Dimensional Connectomics of Anxious Misery, a Human Connectome Study Related to Human Disease: Overview of Protocol and Data Quality. *NeuroImage Clin*. 28: 102489.

21. Costa PT, McCrae RR (1992): *Revised NEO Personality Inventory (NEO PI-R) and NEO Five Factor Inventory: Professional Manual*. *Odessa, FL Psychol Assess Resour*. . doi: 10.1037/0003-066X.52.5.509.

22. Montgomery SA, Asberg M (1979): A new depression scale designed to be sensitive to change. *Br J Psychiatry*. 134: 382–389.

23. HAMILTON M (1960): A rating scale for depression. *J Neurol Neurosurg Psychiatry*. . doi: 10.1136/jnnp.23.1.56.

24. Insel T, Cuthbert BN, Garvey M, Heinssen R, Pine DS, Quinn K, *et al.* (2010): Research Domain Criteria (RDoC): Toward a new classification framework for research on mental disorders. *Am J Psychiatry*. 167: 748–751.

25. Insel TR (2014): The NIMH research domain criteria (RDoC) project: precision medicine for psychiatry. *Am J Psychiatry*. 395–397.

26. Snaith RP, Hamilton M, Morley S, Humayan A, Hargreaves D, Trigwell P (1995): A scale for the assessment of hedonic tone. The Snaith-Hamilton Pleasure Scale. *Br J Psychiatry*. . doi: 10.1192/bjp.167.1.99.

27. Watson D, Clark LA (1991): The mood and anxiety symptom questionnaire (MASQ). *Unpubl manuscript, Univ Iowa, Iowa City*. .

28. Bernstein DP, Fink L (1997): Childhood Trauma Questionnaire: A Retrospective Self-Report (CTQ). *Pearson*. .

29. Bastien CH, Vallières A, Morin CM (2001): Validation of the insomnia severity index as an outcome measure for insomnia research. *Sleep Med*. . doi: 10.1016/S1389-9457(00)00065-4.

30. Loureiro JRA, Leaver A, Vasavada M, Sahib AK, Kubicki A, Joshi S, *et al.* (2020): Modulation of amygdala reactivity following rapidly acting interventions for major depression. *Hum Brain Mapp*. . doi: 10.1002/hbm.24895.

31. Brinker JK, Dozois DJA (2009): Ruminative thought style and depressed mood. *J Clin Psychol*. . doi: 10.1002/jclp.20542.

32. Peterson RA, Heilbronner RL (1987): The anxiety sensitivity index:. Construct validity and factor analytic structure. *J Anxiety Disord*. 1: 117–121.

33. Tozzi L, Staveland B, Holt-Gosselin B, Chesnut M, Chang SE, Choi D, *et al.* (2020): The

human connectome project for disordered emotional states: Protocol and rationale for a research domain criteria study of brain connectivity in young adult anxiety and depression. *Neuroimage*. 214: 116715.

34. Hubbard NA, Siless V, Frosch IR, Goncalves M, Lo N, Wang J, *et al.* (2020): Brain function and clinical characterization in the Boston adolescent neuroimaging of depression and anxiety study. *NeuroImage Clin*. 27. doi: 10.1016/j.nicl.2020.102240.

35. Vasavada MM, Loureiro J, Kubicki A, Sahib A, Wade B, Hellemann G, *et al.* (2020): Effects of Serial Ketamine Infusions on Corticolimbic Functional Connectivity in Major Depression. *Biol Psychiatry Cogn Neurosci Neuroimaging*. . doi: 10.1016/j.bpsc.2020.06.015.

36. Thielscher A, Antunes A, Saturnino GB (2015): Field modeling for transcranial magnetic stimulation: A useful tool to understand the physiological effects of TMS? *Proc Annu Int Conf IEEE Eng Med Biol Soc EMBS*. 222–225.

37. Thielscher A, Opitz A, Windhoff M (2011): Impact of the gyral geometry on the electric field induced by transcranial magnetic stimulation. *Neuroimage*. 54: 234–243.

38. Balderston NL, Roberts C, Beydler EM, Deng Z De, Radman T, Luber B, *et al.* (2020): A generalized workflow for conducting electric field–optimized, fMRI-guided, transcranial magnetic stimulation. *Nat Protoc*. 15: 3595–3614.

39. Glasser MF, Sotiropoulos SN, Wilson JA, Coalson TS, Fischl B, Andersson JL, *et al.* (2013): The minimal preprocessing pipelines for the Human Connectome Project. *Neuroimage*. . doi: 10.1016/j.neuroimage.2013.04.127.

40. Ciric R, Rosen AFG, Erus G, Cieslak M, Adebimpe A, Cook PA, *et al.* (2018): Mitigating head motion artifact in functional connectivity MRI. *Nat Protoc*. . doi: 10.1038/s41596-

018-0065-y.

41. Cox RW (1996): AFNI: software for analysis and visualization of functional magnetic resonance neuroimages. *Comput Biomed Res*. 29: 162–173.

42. Biswal BB, Mennes M, Zuo XN, Gohel S, Kelly C, Smith SM, *et al.* (2010): Toward discovery science of human brain function. *Proc Natl Acad Sci U S A*. . doi: 10.1073/pnas.0911855107.

43. Satterthwaite TD, Elliott MA, Gerraty RT, Ruparel K, Loughead J, Calkins ME, *et al.* (2013): An improved framework for confound regression and filtering for control of motion artifact in the preprocessing of resting-state functional connectivity data. *Neuroimage*. . doi: 10.1016/j.neuroimage.2012.08.052.

44. Smith SM, Brady JM (1997): SUSAN - A new approach to low level image processing. *Int J Comput Vis*. . doi: 10.1023/A:1007963824710.

45. Gordon EM, Laumann TO, Adeyemo B, Huckins JF, Kelley WM, Petersen SE (2016): Generation and Evaluation of a Cortical Area Parcellation from Resting-State Correlations. *Cereb Cortex*. 26: 288–303.

46. Balderston NL, Liu J, Roberson-Nay R, Ernst M, Grillon C (2017): The relationship between dlPFC activity during unpredictable threat and CO<inf>2</inf>-induced panic symptoms. *Transl Psychiatry*. 7. doi: 10.1038/s41398-017-0006-5.

47. Jolliffe IT (1982): A Note on the Use of Principal Components in Regression. *Appl Stat*. . doi: 10.2307/2348005.

48. Sripada C, Angstadt M, Rutherford S, Kessler D, Kim Y, Yee M, Levina E (2019): Basic Units of Inter-Individual Variation in Resting State Connectomes. *Sci Rep*. 9: 1–12.

49. Fox MD, Liu H, Pascual-Leone A (2013): Identification of reproducible individualized

targets for treatment of depression with TMS based on intrinsic connectivity. *Neuroimage*. 66: 151–160.

50. Fox MD, Buckner RL, White MP, Greicius MD, Pascual-Leone A (2012): Efficacy of transcranial magnetic stimulation targets for depression is related to intrinsic functional connectivity with the subgenual cingulate. *Biol Psychiatry*. 72: 595–603.

51. Tao Q, Yang Y, Yu H, Fan L, Luan S, Zhang L, *et al.* (2020): Anatomical Connectivity-Based Strategy for Targeting Transcranial Magnetic Stimulation as Antidepressant Therapy. *Front Psychiatry*. 11: 1–8.

52. Siddiqi SH, Trapp NT, Hacker CD, Laumann TO, Kandala S, Hong X, *et al.* (2019): Repetitive Transcranial Magnetic Stimulation with Resting-State Network Targeting for Treatment-Resistant Depression in Traumatic Brain Injury: A Randomized, Controlled, Double-Blinded Pilot Study. *J Neurotrauma*. 36: 1361–1374.

53. Weigand A, Horn A, Caballero R, Cooke D, Stern AP, Taylor SF, *et al.* (2018): Prospective Validation That Subgenual Connectivity Predicts Antidepressant Efficacy of Transcranial Magnetic Stimulation Sites. *Biol Psychiatry*. 84: 28–37.

54. Cash RFH, Zalesky A, Thomson RH, Tian Y, Cocchi L, Fitzgerald PB (2019): Subgenual Functional Connectivity Predicts Antidepressant Treatment Response to Transcranial Magnetic Stimulation: Independent Validation and Evaluation of Personalization. *Biol Psychiatry*. 86: 2018–2020.

55. Moreno-Ortega M, Kangarlu A, Lee S, Perera T, Kangarlu J, Palomo T, *et al.* (2020): Parcel-guided rTMS for depression. *Transl Psychiatry*. 10. doi: 10.1038/s41398-020-00970-8.

56. Fox MD, Halko MA, Eldaief MC, Pascual-Leone A (2012): Measuring and manipulating brain connectivity with resting state functional connectivity magnetic resonance imaging

(fcMRI) and transcranial magnetic stimulation (TMS). *Neuroimage*. 62: 2232–2243.

57. Cash RFH, Weigand A, Zalesky A, Siddiqi SH, Downar J, Fitzgerald PB, Fox MD (2020): Using Brain Imaging to Improve Spatial Targeting of Transcranial Magnetic Stimulation for Depression. *Biol Psychiatry*. 1–12.
58. Cash RFH, Cocchi L, Lv J, Fitzgerald PB, Zalesky A (2020): Functional Magnetic Resonance Imaging-Guided Personalization of Transcranial Magnetic Stimulation Treatment for Depression. *JAMA psychiatry*. 1–3.
59. Singh A, Erwin-Grabner T, Sutcliffe G, Antal A, Paulus W, Goya-Maldonado R (2019): Personalized repetitive transcranial magnetic stimulation temporarily alters default mode network in healthy subjects. *Sci Rep*. 9: 1–12.
60. Liston C, Chen AC, Zebley BD, Drysdale AT, Gordon R, Leuchter B, *et al.* (2014): Default mode network mechanisms of transcranial magnetic stimulation in depression. *Biol Psychiatry*. 76: 517–526.
61. Beynel L, Powers JP, Appelbaum LG (2020): Effects of repetitive transcranial magnetic stimulation on resting-state connectivity: A systematic review. *Neuroimage*. 211: 116596.
62. Chen FJ, Gu CZ, Zhai N, Duan HF, Zhai AL, Zhang X (2020): Repetitive Transcranial Magnetic Stimulation Improves Amygdale Functional Connectivity in Major Depressive Disorder. *Front Psychiatry*. 11: 1–9.
63. Du L, Liu H, Du W, Chao F, Zhang L, Wang K, *et al.* (2017): Stimulated left DLPFC-nucleus accumbens functional connectivity predicts the anti-depression and anti-anxiety effects of rTMS for depression. *Transl Psychiatry*. 7: 1–9.
64. Avissar M, Powell F, Ilieva I, Respino M, Gunning FM, Liston C, Dubin MJ (2017): Functional connectivity of the left DLPFC to striatum predicts treatment response of

depression to TMS. *Brain Stimul*. 10: 919–925.

65. Yu M, Linn KA, Shinohara RT, Oathes DJ, Cook PA, Duprat R, *et al.* (2019): Childhood trauma history is linked to abnormal brain connectivity in major depression. *Proc Natl Acad Sci*. 116: 8582–8590.

66. Williams LM (2017): Defining biotypes for depression and anxiety based on large-scale circuit dysfunction: a theoretical review of the evidence and future directions for clinical translation. *Depress Anxiety*. . doi: 10.1002/da.22556.

67. Slotema CW, Blom JD, Hoek HW, Sommer IEC (2010): Should we expand the toolbox of psychiatric treatment methods to include repetitive transcranial magnetic stimulation (rTMS)? A meta-analysis of the efficacy of rTMS in psychiatric disorders. *J Clin Psychiatry*. 71: 873–884.

68. Nahas Z, Lomarev M, Roberts DR, Shastri A, Lorberbaum JP, Teneback C, *et al.* (2001): Unilateral left prefrontal transcranial magnetic stimulation (TMS) produces intensity-dependent bilateral effects as measured by interleaved BOLD fMRI. *Biol Psychiatry*. . doi: 10.1016/S0006-3223(01)01199-4.

69. Clarke R, Johnstone T (2013): Prefrontal inhibition of threat processing reduces working memory interference. *Front Hum Neurosci*. 7: 228.

70. Daunizeau J, David O, Stephan KE (2011): Dynamic causal modelling: A critical review of the biophysical and statistical foundations. *Neuroimage*. . doi: 10.1016/j.neuroimage.2009.11.062.

71. Friston KJ, Li B, Daunizeau J, Stephan KE (2011): Network discovery with DCM. *Neuroimage*. . doi: 10.1016/j.neuroimage.2010.12.039.

72. Prando G, Zorzi M, Bertoldo A, Corbetta M, Zorzi M, Chiuso A (2020): Sparse DCM for

whole-brain effective connectivity from resting-state fMRI data. *Neuroimage*. . doi: 10.1016/j.neuroimage.2019.116367.

73. Pascual-Leone A, Tormos JM, Keenan J, Tarazona F, Cañete C, Catalá MD (1998): Study and modulation of human cortical excitability with transcranial magnetic stimulation. *J Clin Neurophysiol*. . doi: 10.1097/00004691-199807000-00005.

74. Chen R, Classen J, Gerloff C, Celnik P, Wassermann EM, Hallett M, Cohen LG (1997): Depression of motor cortex excitability by low-frequency transcranial magnetic stimulation. *Neurology*. . doi: 10.1212/WNL.48.5.1398.

75. Balderston NL, Beydler EM, Roberts C, Deng Z De, Radman T, Lago T, *et al.* (2020): Mechanistic link between right prefrontal cortical activity and anxious arousal revealed using transcranial magnetic stimulation in healthy subjects. *Neuropsychopharmacology*. 45: 694–702.

76. Balderston NL, Beydler EM, Goodwin M, Deng Z De, Radman T, Luber BM, *et al.* (2020): Low-frequency parietal repetitive transcranial magnetic stimulation reduces fear and anxiety. *Transl Psychiatry*. 10. doi: 10.1038/s41398-020-0751-8.

77. Di Lazzaro V, Dileone M, Pilato F, Capone F, Musumeci G, Ranieri F, *et al.* (2011): Modulation of motor cortex neuronal networks by rTMS: comparison of local and remote effects of six different protocols of stimulation. *J Neurophysiol*. 105: 2150–2156.

78. Komssi S, Kähkönen S, Ilmoniemi RJ (2004): The Effect of Stimulus Intensity on Brain Responses Evoked by Transcranial Magnetic Stimulation. *Hum Brain Mapp*. . doi: 10.1002/hbm.10159.

79. Chen J, Zhou C, Wu B, Wang Y, Li Q, Wei Y, *et al.* (2013): Left versus right repetitive transcranial magnetic stimulation in treating major depression: A meta-analysis of

randomised controlled trials. *Psychiatry Res*. 210: 1260–1264.

80. Huang YZ, Edwards MJ, Rounis E, Bhatia KP, Rothwell JC (2005): Theta burst stimulation of the human motor cortex. *Neuron*. 45: 201–206.

Appendix: Equations

Connectivity based model: PCA regression

Let $\mathbf{Y}^{mood}$ be the $n \times 1$ vector of behavioral symptom scores (e.g., MADRS scores) for n participants. We assume the behavioral symptom scores can be predicted using a linear combination of connectivity measures, according to the model

$$\boldsymbol{Y}^{mood} = \boldsymbol{X}\boldsymbol{\beta} + \boldsymbol{\epsilon},$$

where $\boldsymbol{X}$ is a $n \times p$ matrix such that each row consists of one participant's concatenated unique connectivity values from the Z-transformed Pearson correlation functional connectivity matrix, i.e., the upper or lower triangular portion of the $N \times N$ connectivity matrix ($p = N(N-1)/2$), for the Gordon atlas, $N = 333$); $\boldsymbol{\beta}$ is a $p \times 1$ vector of coefficients, and $\boldsymbol{\epsilon}$ is a $n \times 1$ vector of error terms. We assume that $\boldsymbol{Y}^{mood}$ and columns of $\boldsymbol{X}$ have been centered so as to have zero empirical means.

We perform principal components analysis (PCA) on the predictor matrix $\boldsymbol{X}$. Let $\boldsymbol{X} = \boldsymbol{U}\boldsymbol{\Delta}\boldsymbol{V}^{\boldsymbol{T}}$ denote the singular value decomposition of $\boldsymbol{X}$, where $\boldsymbol{\Delta}_{p\times p} = \mathrm{diag}(\delta_1, \dots, \delta_p)$ is a diagonal matrix of non-negative singular values, and columns of $\boldsymbol{U}_{n\times p}$ and $\boldsymbol{V}_{p\times p}$ are orthonormal sets of vectors, i.e., the left and right singular vectors of $\boldsymbol{X}$. The spectral decomposition of $\boldsymbol{X}$ is given by $\boldsymbol{V}\boldsymbol{\Lambda}\boldsymbol{V}^{\boldsymbol{T}}$, where $\boldsymbol{\Lambda}_{p\times p} = \mathrm{diag}(\lambda_1, \dots, \lambda_p) = \mathrm{diag}(\delta_1^2, \dots, \delta_p^2) = \boldsymbol{\Delta}^2$ is a diagonal matrix of the non-negative eigenvalues of $\boldsymbol{X}^{\boldsymbol{T}}\boldsymbol{X}$ and columns of $\boldsymbol{V}_{p\times p} = [\boldsymbol{v_1}, \dots, \boldsymbol{v_p}]$ are the corresponding eigenvectors. The jth principal component and jth principal component direction (i.e., PCA loading) corresponding to the jth largest eigenvector are $\boldsymbol{X}\boldsymbol{v_j}$ and $\boldsymbol{v_j}$, respectively, for each $j \in \{1, \dots, p\}$.

For PCA regression (PCR), we use the first $k \leq n$ components as predictors. Let $\boldsymbol{V}_k$ represent the $p \times k$ matrix comprising the first k columns of $\boldsymbol{V}$, and $\boldsymbol{W}_k = \boldsymbol{X}\boldsymbol{V}_k$ be the $n \times k$ matrix with the first k principal components as columns. We estimate regression coefficients $\boldsymbol{\gamma}_k$ in $\boldsymbol{Y}^{mood} = \boldsymbol{W}_k\boldsymbol{\gamma}_k + \boldsymbol{\epsilon}_k$ by ordinary least squares, i.e., $\boldsymbol{\gamma}_k = (\boldsymbol{W}_k^T\boldsymbol{W}_k)^{-1}\boldsymbol{W}_k^T\boldsymbol{Y}^{mood} \in \mathbb{R}^k$. Then the PCR estimator of $\boldsymbol{\beta}$ based on the first k principal components is given by $\widehat{\boldsymbol{\beta}}_k = \boldsymbol{V}_k\widehat{\boldsymbol{\gamma}}_k \in \mathbb{R}^p$.

E-field augmented model

Once $\widehat{\boldsymbol{\beta}}_k$ is obtained from the connectivity based model, the e-field augmented model will be used to identify the optimal coil orientation and stimulation sites to generate the greatest reduction in behavioral symptom score for each participant. Let $\Delta\boldsymbol{Y}^{mood}$ be the $n \times 1$ vector of changes in score between the pre- and post-treatment assessments for n participants. We model $\Delta\boldsymbol{Y}^{mood}$ as follows:

$$\Delta\boldsymbol{Y}^{mood} = \boldsymbol{Y}_{post}^{mood} - \boldsymbol{Y}_{pre}^{mood} = (\boldsymbol{X}_{post} - \boldsymbol{X}_{pre})\boldsymbol{\beta} + \boldsymbol{\epsilon}',$$

where $\boldsymbol{\epsilon}' = \boldsymbol{\epsilon}_{post} - \boldsymbol{\epsilon}_{pre}$.

For each site and orientation l, let $\boldsymbol{E}_l$ be a $n \times p$ matrix, where rows correspond to participants,

columns correspond to pairs of regions in the Gordon atlas, and entries equal the average e-field model values at each pair of regions for the given participant, site, and orientation. We assume that $\boldsymbol{X}_{post}^{l} = C \cdot \boldsymbol{E}_l \circ \boldsymbol{X}_{pre}$, where C is a positive proportionality constant, and $\circ$ denotes the Hadamard product. Thus, for a given stimulation site and coil orientation combination l,

$$\Delta \boldsymbol{Y}^{mood} = \left(C \cdot \boldsymbol{E}_l \circ \boldsymbol{X}_{pre} - \boldsymbol{X}_{pre}\right)\boldsymbol{\beta} + \boldsymbol{\epsilon}'.$$

With these assumptions, and substituting the $\widehat{\boldsymbol{\beta}}_k$ estimated form the PCR described above, it is possible to compare relative differences in the predicted change in behavioral symptom score across sites and orientations l.

Table 1: Demographic information and clinical measures

	AM	Control
Demographic Information		
Age	28.29 (8.2)	28.92 (6.91)
Females	64	16
Clinical measures		
HAMD	13.3 (5.67)	1.28 (1.93)
MADRS	21.08 (8.87)	0.68 (1.18)
SHAPS	41.24 (7.61)	51.28 (5.37)
MASQ	60.35 (9.07)	48.76 (12.21)
CTQ	62.53 (8.79)	61.04 (5.77)
ISI	11.86 (6.12)	3.28 (3.27)
RTS	95.09 (21.51)	48.2 (21.07)
ASI	28.13 (14.71)	6.72 (5.91)

Table 2: Sites used to define the P --> A dlPFC axis

Site	x		y	z	Location Details
	Left	Right			
1	-43.5	43.5	4.5	59.5	Most posterior
2	-42.7	42.7	8.3	57.7	
3	-41.8	41.8	12.2	55.8	
4	-41.0	41.0	16.0	54.0	5 cm therapeutic site
5	-40.2	40.2	19.8	52.2	
6	-39.3	39.3	23.7	50.3	
7	-38.5	38.5	27.5	48.5	
8	-37.7	37.7	31.3	46.7	
9	-36.8	36.8	35.2	44.8	
10	-36.0	36.0	39.0	43.0	BA9
11	-38.0	38.0	39.3	39.5	
12	-40.0	40.0	39.5	36.0	
13	-42.0	42.0	39.8	32.5	
14	-44.0	44.0	40.0	29.0	BA46
15	-46.0	46.0	40.3	25.5	
16	-48.0	48.0	40.5	22.0	
17	-50.0	50.0	40.8	18.5	Most Anterior

Table 2: Permutation test thresholds

Clinical Measures	AM		Control	
	Left	Right	Left	Right
MADRS	2.44	2.49	2.56	2.56
HAMD	2.47	2.49	2.6	2.62
Loss	2.42	2.44	2.42	2.43

Figure Legends

Figure 1. Theoretical basis for current model. A) Depicts a basic linear relationship between a hypothetical symptom and a hypothetical functional connection in the brain. **B**) Depicts a revised equation where the slope of the relationship is modified by a weighting factor "E", which represents the change in connectivity induced by a TMS treatment, estimated from the electric (e)-field model.

Figure 2. The PCA-Regression data reduction approach used to summarize the relationship between symptoms and connectivity in the current model. A) Resting state functional connectivity (rsFC) is calculated using Pearson's correlations across all subjects for all regions in the Gordon atlas (45). **B**) A Principal component analysis is used to identify orthogonal components in the rsFC data, and a geometric approach is used to identify a minimal number of components that explain a maximal proportion of the variability. **C)** Component scores for the selected components are extracted and entered into a multiple linear regression to predict symptoms (**D**). The item coefficients from the selected components (**E**) are combined with the beta vector from the regression (**F**) using matrix multiplication to create the output vector (**G**), which is used to represent the slope of the line relating connectivity and symptoms.

Figure 3. Methods used to summarize electric (e)-field models in NxN connectivity space. Normalized e-field models were first downsampled to the Gordon atlas (45). The results were then converted to a 1 x N vector. This vector was then rotated by 90 degrees, averaged, and thresholded to create an N x N matrix with the same dimensions and sorting as the rsFC matricies.

Figure 4. Iteration of model across site and orientation. To understand how placement and orientation of the TMS coil might impact symptoms, we computed our model across multiple sites and orientations. Sites were defined at equally spaced points along the anterior to posterior axis of the middle frontal gyrus. Roll and pitch were defined orthogonal to the scalp at each stimulation site. Multiple equally spaced yaw vectors were defined at each stimulation site, representing all possible coil orientations. Electric (e)-field models were conducted at each site/orientation combination, entered into our symptom prediction model, and the results were plotted in this site x orientation heatmap.

Figure 5. Individual subject data for the anxious misery group. (**A, C, E, G**) Heatmaps representing the predicted MADRS scores following a hypothetical course of TMS treatment to the left dlPFC. (**B, D, F, H**) Heatmaps representing the predicted MADRS scores following a hypothetical course of TMS treatment to the right dlPFC. Colors represent the predicted MADRS scores. Y axis represents coil orientation. X axis represents location along the Z-axis of the middle frontal gyrus. "X" in heatmaps represent the site and orientation of stimulation predicted to have the maximal reduction in symptoms for each subject.

Figure 6. Individual subject data for the healthy control group. (**A, C, E, G**) Heatmaps representing the predicted MADRS scores following a hypothetical course of TMS treatment to the left dlPFC. (**B, D, F, H**) Heatmaps representing the predicted MADRS scores following a hypothetical course of TMS treatment to the right dlPFC. Colors represent the predicted MADRS scores. Y axis represents coil orientation. X axis represents location along the Z-axis of the middle frontal gyrus. “X” in heatmaps represent the site and orientation of stimulation predicted to have the maximal reduction in symptoms for each subject.

Figure 7. Group-level data for the anxious misery group. A) Heatmap representing the predicted MADRS scores following a hypothetical course of TMS treatment to the left dlPFC. **B**) Heatmap representing the predicted MADRS scores following a hypothetical course of TMS treatment to the right dlPFC. **C**) Heatmap representing the predicted HAMD scores following a hypothetical course of TMS treatment to the left dlPFC. **D**) Heatmap representing the predicted HAMD scores following a hypothetical course of TMS treatment to the right dlPFC. **E**) Heatmap representing the predicted Loss cluster scores following a hypothetical course of TMS treatment to the left dlPFC. **F**) Heatmap representing the predicted Loss cluster scores following a hypothetical course of TMS treatment to the right dlPFC. Heatmaps representing the predicted MADRS scores following a hypothetical course of TMS treatment to the right dlPFC. Colors represent the predicted MADRS scores. Y axis represents coil orientation. X axis represents location along the Z-axis of the middle frontal gyrus. “X” in heatmaps represent the site and orientation of stimulation predicted to have the maximal reduction in symptoms across the group. Diagonal hatching represents sites where the change in MADRS/HAMD scores was not statistically different from 0.

Figure 8. Group-level data for the healthy control group. A) Heatmap representing the predicted MADRS scores following a hypothetical course of TMS treatment to the left dlPFC. **B**) Heatmap representing the predicted MADRS scores following a hypothetical course of TMS treatment to the right dlPFC. **C**) Heatmap representing the predicted HAMD scores following a hypothetical course of TMS treatment to the left dlPFC. **D**) Heatmap representing the predicted HAMD scores following a hypothetical course of TMS treatment to the right dlPFC. **E**) Heatmap representing the predicted Loss cluster scores following a hypothetical course of TMS treatment to the left dlPFC. **F**) Heatmap representing the predicted Loss cluster scores following a hypothetical course of TMS treatment to the right dlPFC. Heatmaps representing the predicted MADRS scores following a hypothetical course of TMS treatment to the right dlPFC. Colors represent the predicted MADRS scores. Y axis represents coil orientation. X axis represents location along the Z-axis of the middle frontal gyrus. “X” in heatmaps represent the site and orientation of stimulation predicted to have the maximal reduction in symptoms across the group. Diagonal hatching represents sites where the change in MADRS/HAMD scores was not statistically different from 0.

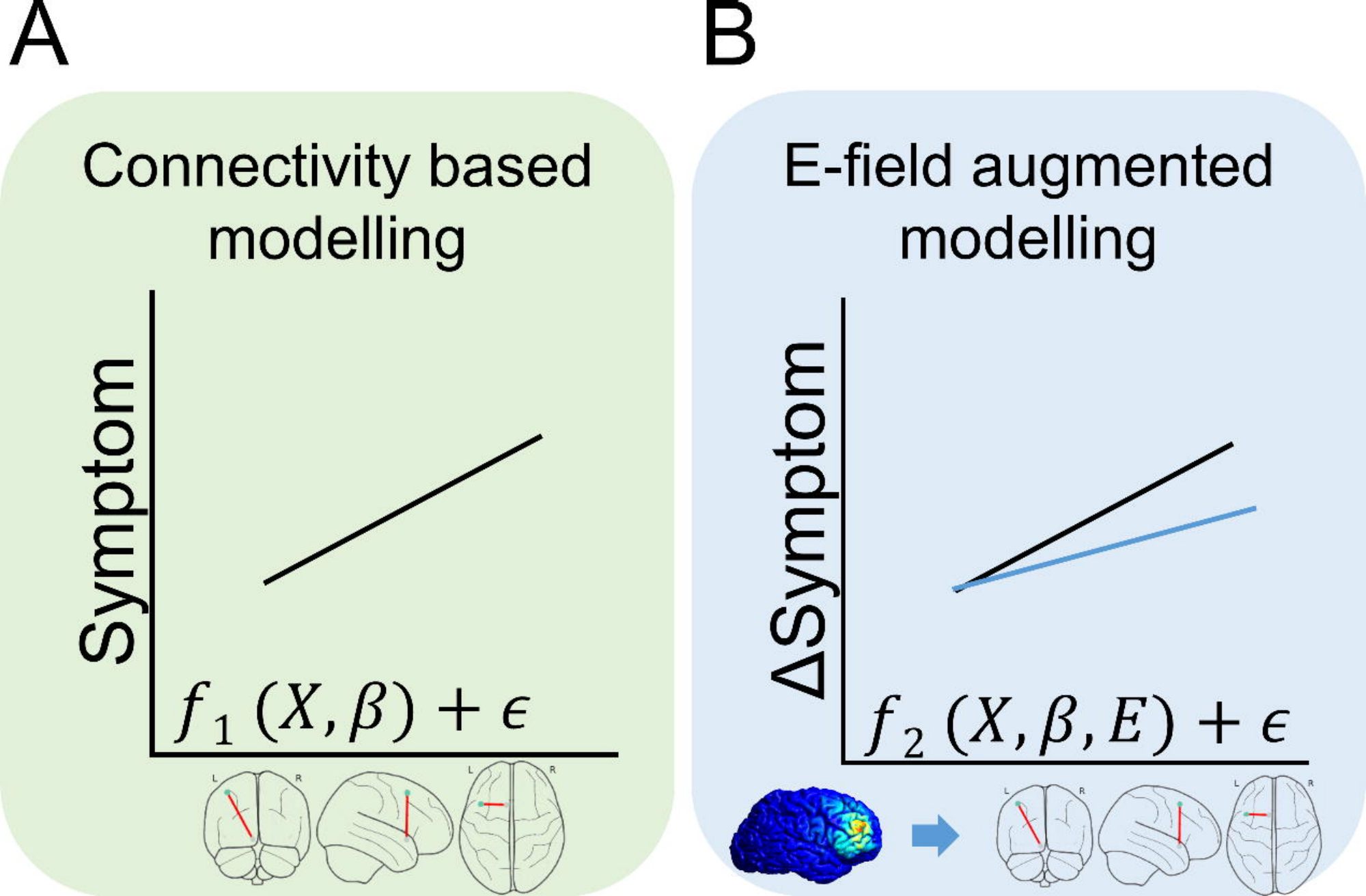
A
Connectivity based modelling
Symptom
$f_1(X, \beta) + \epsilon$
B
E-field augmented modelling
ΔSymptom
$f_2(X, \beta, E) + \epsilon$

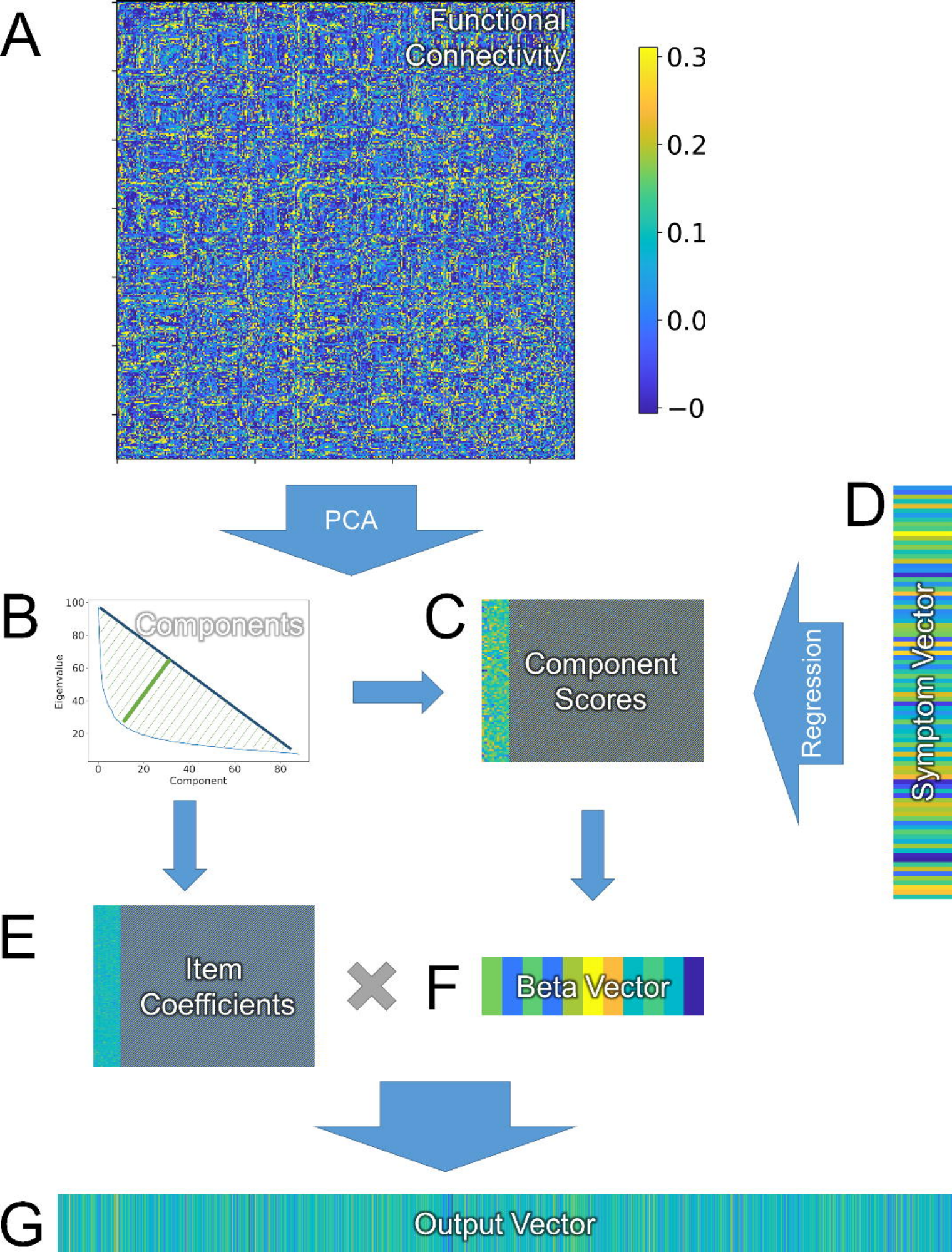
A
Functional Connectivity
0.3
0.2
0.1
0.0
−0
PCA
B
Components
Eigenvalue
Component
C
Component Scores
Regression
D
Symptom Vector
E
Item Coefficients
F
Beta Vector
G
Output Vector

Scale models to whole brain using Gordon atlas

Reshape e-field to match N x N connectivity graph

Compute e-field → Downsample to atlas → Vectorize results → Convert to graph

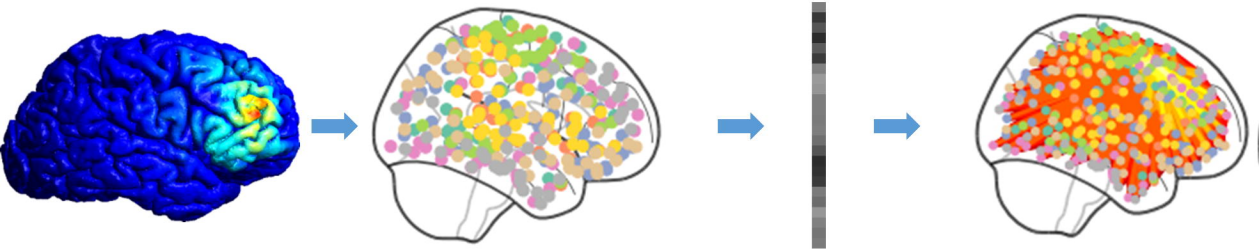

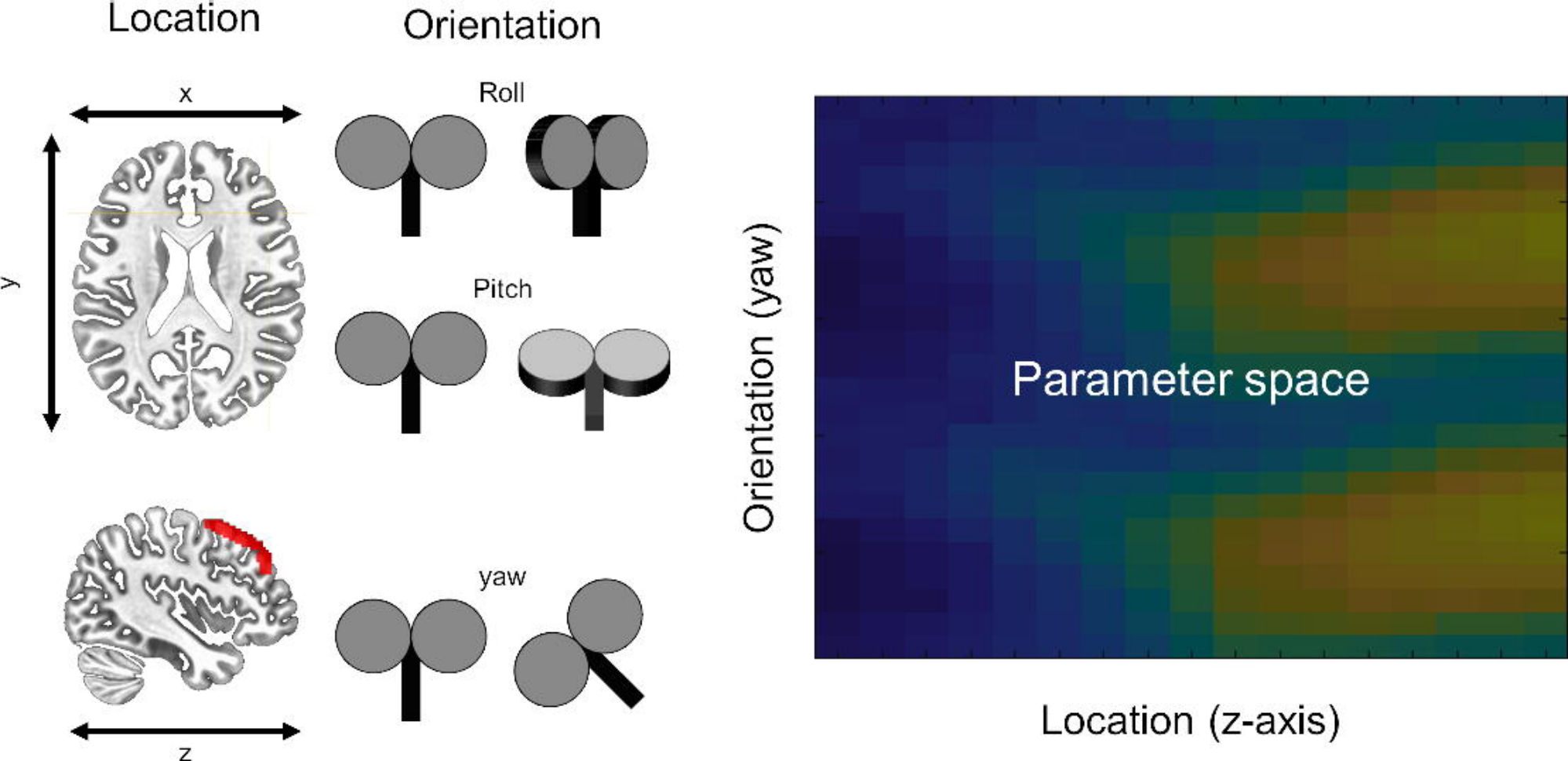
Location
Orientation
x
y
z
Roll
Pitch
yaw
Parameter space
Orientation (yaw)
Location (z-axis)

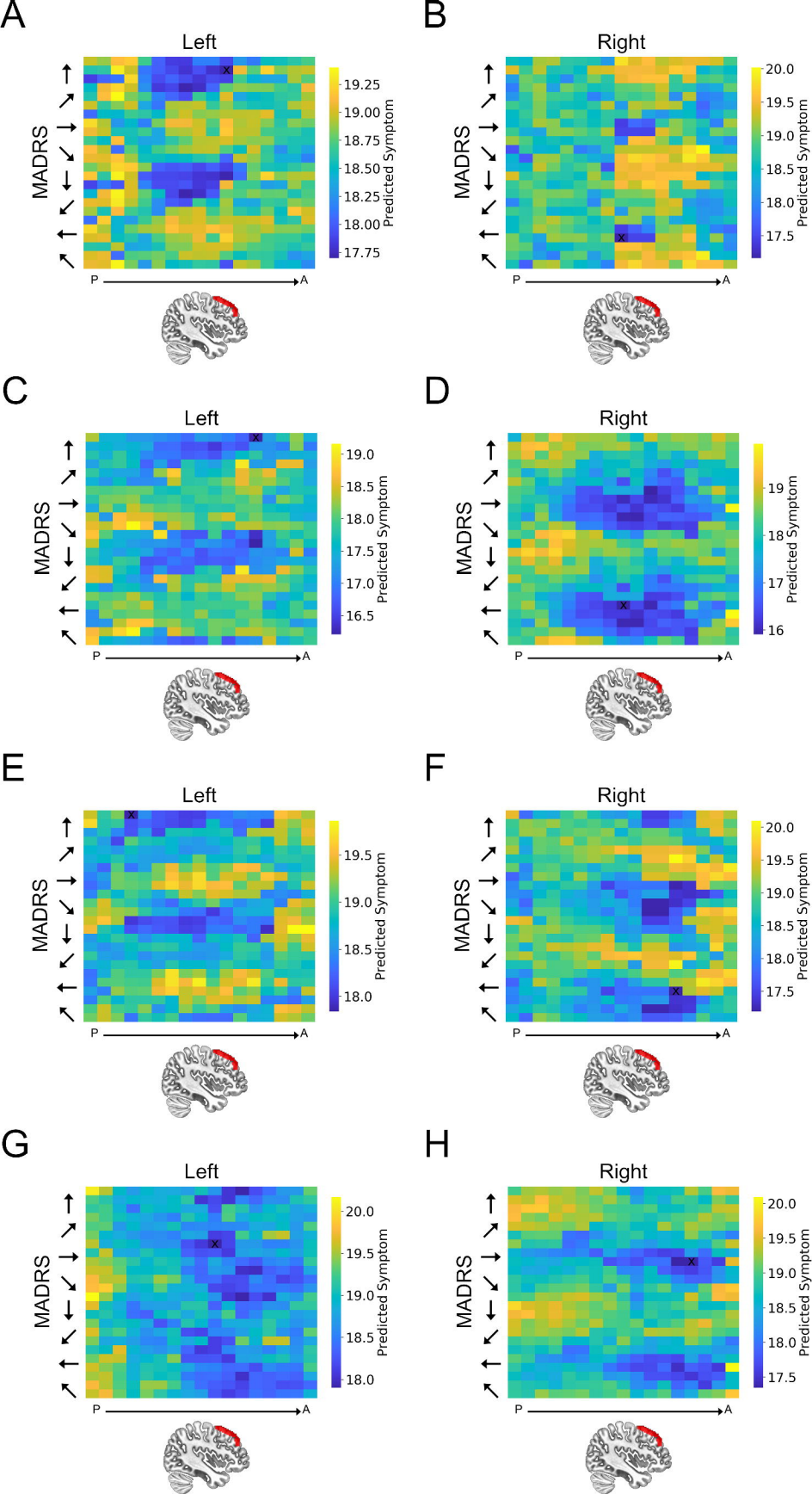
A
Left
MADRS
P
A
19.25
19.00
18.75
18.50
18.25
18.00
17.75
Predicted Symptom
B
Right
MADRS
P
A
20.0
19.5
19.0
18.5
18.0
17.5
Predicted Symptom
C
Left
MADRS
P
A
19.0
18.5
18.0
17.5
17.0
16.5
Predicted Symptom
D
Right
MADRS
P
A
19
18
17
16
Predicted Symptom
E
Left
MADRS
P
A
19.5
19.0
18.5
18.0
Predicted Symptom
F
Right
MADRS
P
A
20.0
19.5
19.0
18.5
18.0
17.5
Predicted Symptom
G
Left
MADRS
P
A
20.0
19.5
19.0
18.5
18.0
Predicted Symptom
H
Right
MADRS
P
A
20.0
19.5
19.0
18.5
18.0
17.5
Predicted Symptom

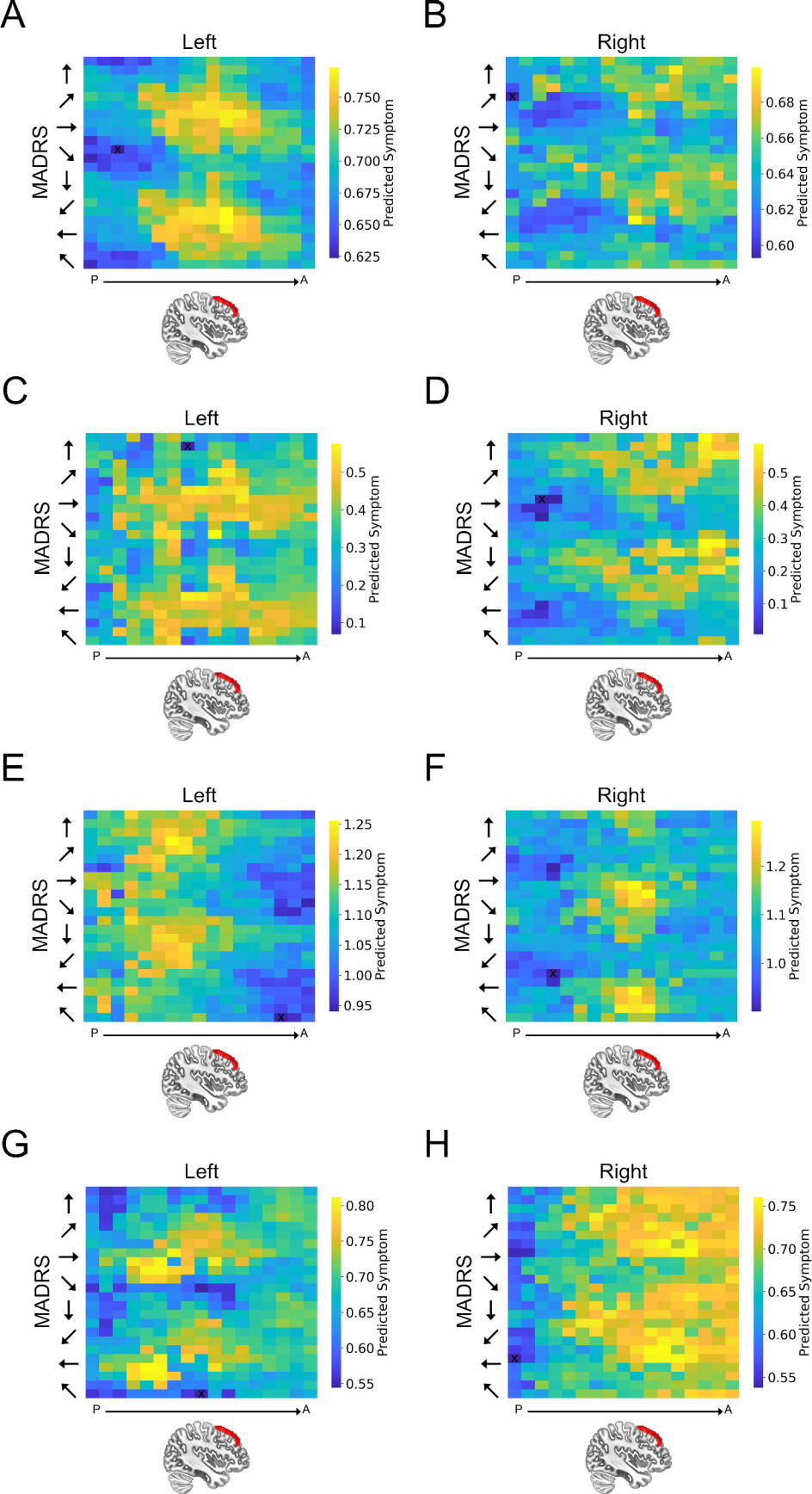
A
Left
MADRS
P
A
0.750
0.725
0.700
0.675
0.650
0.625
Predicted Symptom
B
Right
MADRS
P
A
0.68
0.66
0.64
0.62
0.60
Predicted Symptom
C
Left
MADRS
P
A
0.5
0.4
0.3
0.2
0.1
Predicted Symptom
D
Right
MADRS
P
A
0.5
0.4
0.3
0.2
0.1
Predicted Symptom
E
Left
MADRS
P
A
1.25
1.20
1.15
1.10
1.05
1.00
0.95
Predicted Symptom
F
Right
MADRS
P
A
1.2
1.1
1.0
Predicted Symptom
G
Left
MADRS
P
A
0.80
0.75
0.70
0.65
0.60
0.55
Predicted Symptom
H
Right
MADRS
P
A
0.75
0.70
0.65
0.60
0.55
Predicted Symptom

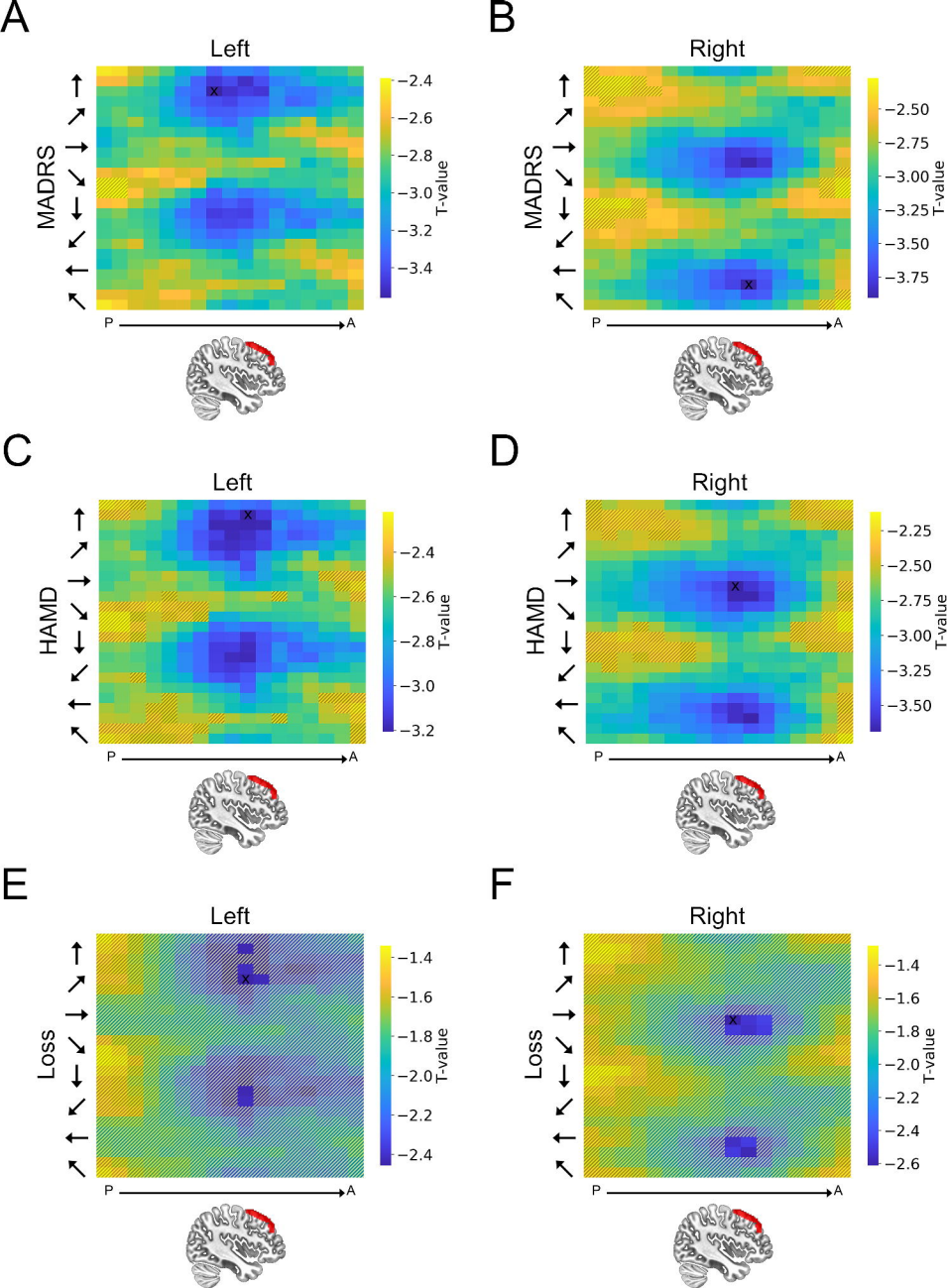
A
Left
MADRS
−2.4
−2.6
−2.8
−3.0
−3.2
−3.4
T-value
P
A
B
Right
MADRS
−2.50
−2.75
−3.00
−3.25
−3.50
−3.75
T-value
P
A
C
Left
HAMD
−2.4
−2.6
−2.8
−3.0
−3.2
T-value
P
A
D
Right
HAMD
−2.25
−2.50
−2.75
−3.00
−3.25
−3.50
T-value
P
A
E
Left
Loss
−1.4
−1.6
−1.8
−2.0
−2.2
−2.4
T-value
P
A
F
Right
Loss
−1.4
−1.6
−1.8
−2.0
−2.2
−2.4
−2.6
T-value
P
A

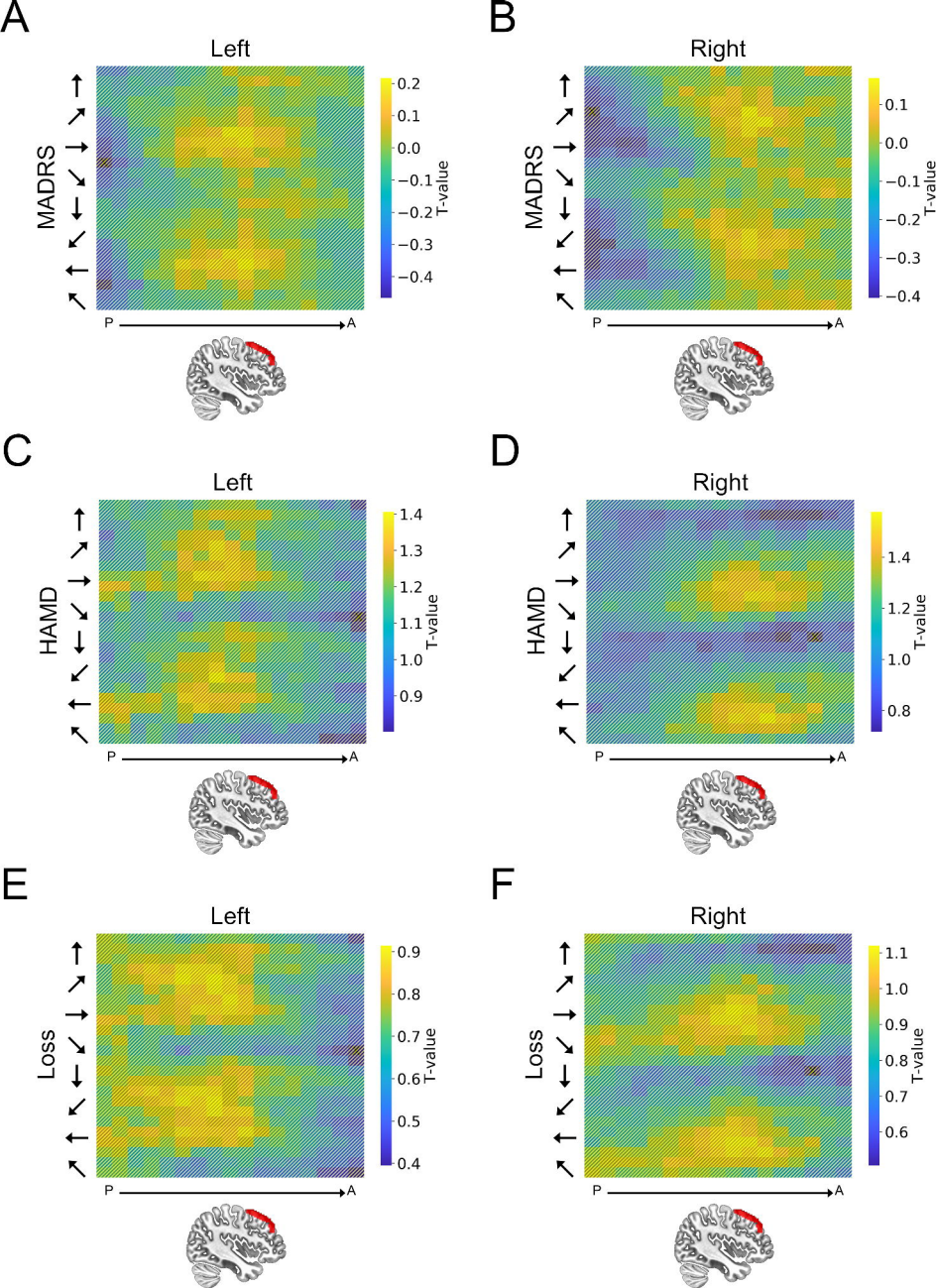
A
Left
MADRS
0.2
0.1
0.0
−0.1
−0.2
−0.3
−0.4
T-value
P
A
B
Right
MADRS
0.1
0.0
−0.1
−0.2
−0.3
−0.4
T-value
P
A
C
Left
HAMD
1.4
1.3
1.2
1.1
1.0
0.9
T-value
P
A
D
Right
HAMD
1.4
1.2
1.0
0.8
T-value
P
A
E
Left
Loss
0.9
0.8
0.7
0.6
0.5
0.4
T-value
P
A
F
Right
Loss
1.1
1.0
0.9
0.8
0.7
0.6
T-value
P
A